

Article

Energy and Electronic Properties of Nanostructures Based on the CL-20 Framework with the Replacement of the Carbon Atoms by Silicon and Germanium: A Density Functional Theory Study

Margarita A. Gimaldinova¹, Mikhail M. Maslov^{1,2,*}  and Konstantin P. Katin^{1,2} 

¹ Nanoengineering in Electronics, Spintronics and Photonics Institute, National Research Nuclear University “MEPhI”, Kashirskoe Shosse 31, 115409 Moscow, Russia

² Laboratory of Computational Design of Nanostructures, Nanodevices, and Nanotechnologies, Research Institute for the Development of Scientific and Educational Potential of Youth, Aviatorov Str. 14/55, 119620 Moscow, Russia

* Correspondence: mike.maslov@gmail.com

Abstract: We consider $\text{Si}_n\text{CL-20}$ and $\text{Ge}_n\text{CL-20}$ systems with carbon atoms replaced by silicon/germanium atoms and their dimers. The physicochemical properties of the silicon/germanium analogs of the high-energy molecule CL-20 and its dimers were determined and studied using density functional theory with the B3LYP/6-311G(d,p) level of theory. It was found that the structure and geometry of $\text{Si}_n\text{CL-20}/\text{Ge}_n\text{CL-20}$ molecules change dramatically with the appearance of Si-/Ge-atoms. The main difference between silicon- or germanium-substituted $\text{Si}_n\text{CL-20}/\text{Ge}_n\text{CL-20}$ molecules and the pure CL-20 molecule is that the NO_2 functional groups make a significant rotation relative to the starting position in the classical molecule, and the effective diameter of the frame of the systems increases with the addition of Si-/Ge-atoms. Thus, the effective framework diameter of a pure CL-20 molecule is 3.208 Å, while the effective diameter of a fully silicon-substituted $\text{Si}_6\text{CL-20}$ molecule is 4.125 Å, and this parameter for a fully germanium-substituted $\text{Ge}_6\text{CL-20}$ molecule is 4.357 Å. The addition of silicon/germanium atoms to the system leads to a decrease in the binding energy. In detail, the binding energies for CL-20/ $\text{Si}_6\text{CL-20}/\text{Ge}_6\text{CL-20}$ molecules are 4.026, 3.699, 3.426 eV/atom, respectively. However, it has been established that the framework maintains stability, with an increase in the number of substituting silicon or germanium atoms. In addition, we designed homodesmotic reactions for the CL-20 molecule and its substituted derivatives $\text{Si}_6\text{CL-20}/\text{Ge}_6\text{CL-20}$, and then determined the strain energy to find out in which case more energy would be released when the framework breaks. Further, we also studied the electronic properties of systems based on CL-20 molecules. It was found that the addition of germanium or silicon atoms instead of carbon leads to a decrease in the size of the HOMO–LUMO gap. Thus, the HOMO–LUMO gaps of the CL-20/ $\text{Si}_6\text{CL-20}/\text{Ge}_6\text{CL-20}$ molecules are 5.693, 5.339, and 5.427 eV, respectively. A similar dependence is also observed for CL-20 dimers. So, in this work, we have described in detail the dependence of the physicochemical parameters of CL-20 molecules and their dimers on the types of atoms upon substitution.

Keywords: high-energy molecules; CL-20; density functional theory; chemical reactivity; strain energy; covalent dimers



Citation: Gimaldinova, M.A.; Maslov, M.M.; Katin, K.P. Energy and Electronic Properties of Nanostructures Based on the CL-20 Framework with the Replacement of the Carbon Atoms by Silicon and Germanium: A Density Functional Theory Study. *Materials* **2022**, *15*, 6577. <https://doi.org/10.3390/ma15196577>

Academic Editor: Francisco Carrasco-Marín

Received: 31 August 2022

Accepted: 19 September 2022

Published: 22 September 2022

Publisher's Note: MDPI stays neutral with regard to jurisdictional claims in published maps and institutional affiliations.



Copyright: © 2022 by the authors. Licensee MDPI, Basel, Switzerland. This article is an open access article distributed under the terms and conditions of the Creative Commons Attribution (CC BY) license (<https://creativecommons.org/licenses/by/4.0/>).

1. Introduction

The isolated molecule CL-20, also known as hexanitrohexaazaisowurtzitane ($\text{C}_6\text{H}_6\text{N}_{12}\text{O}_{12}$), was synthesized in California in 1987 [1]. It is representative of the class of high-energy-density materials (HEDMs) [2], and its unique properties are due to its unusual size and shape. Isolated CL-20 is formed by a strained carbon–nitrogen framework consisting of two five-membered and one six-membered ring connected by C–C bonds and six NO_2 functional

groups attached to this framework. Figure 1a illustrates the molecular structure of the $C_6H_6N_{12}O_{12}$. Hexanitrohexaazaisowurtzitane (CL-20) is the most promising HEDM at present and exhibits better comprehensive properties than most high-energy materials [3].

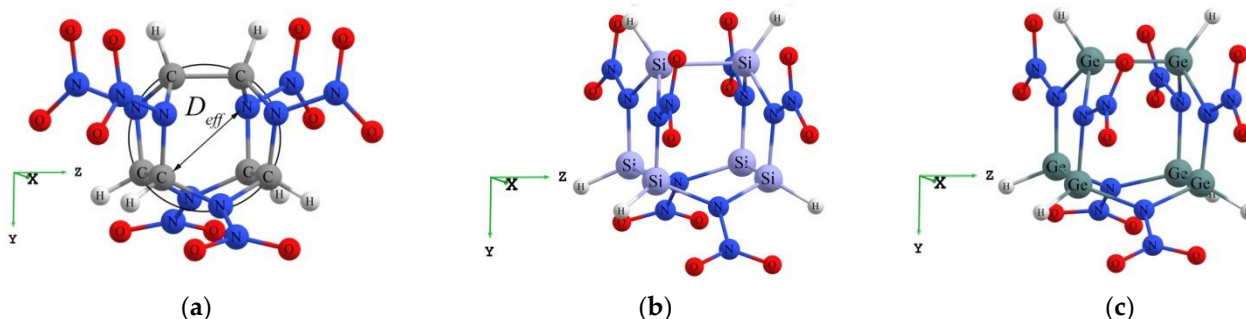


Figure 1. (a)—The isolated molecule CL-20; (b)—the isolated molecule Si_6CL-20 ; (c)—the isolated molecule Ge_6CL-20 .

Previously, nanostructures based on hexanitrohexaazaisowurtzitane were created by various methods to improve the properties of these compounds, such as composition density, thermal stability, and others. Despite the fact that CL-20 is a metastable compound, it can form molecular crystals, in which separate CL-20 molecules retain their individuality [4–6]. Moreover, currently, the cocrystallization method is widely applied to various high-energy materials including CL-20. A large number of molecular cocrystals based on CL-20 were obtained, and their properties were studied, for example, TNT/CL-20 [7–10], HMX/CL-20 [7,8], CL-20/DNT [11], CL-20/RDX [12], etc.

Then, for the first time, a molecule-based covalent CL-20 crystal was predicted using computer simulation. One-dimensional CL-20 chains have been constructed using CH_2 molecular bridges for the covalent bonding between the isolated CL-20 fragments. It was found that such systems become more thermodynamically stable as their efficient length increases [13]. It is confirmed that the use of CH_2 bridges is the universal technique to connect both CL-20 fragments in the chain and the chains together to make a network. In the previous study [14], we analyzed the properties of the quasi-one-dimensional and quasi-two-dimensional systems consisting of CL-20 molecules. Covalent crystals have several advantages over molecular ones since they have a higher density along with higher kinetic stability. Thus, the formation of bulk covalent CL-20 solids may be energetically favourable.

Furthermore, it is known that carbon-based compounds can successfully exist even if carbon atoms are replaced by their closest analogues in the periodic table—silicon and germanium. Silicon and germanium are similar to carbon in some chemical properties. The successful replacement of carbon atoms with silicon and germanium atoms is found in various applications. Thus, organic cells with carbon-silicon chemical bonds were obtained using a live biocatalyst [15]. In research on new drugs, carbon is replaced by silicon [16]. Chemistry also uses organic polymers based on silicon [17]. They are used in agriculture and the semiconductor industry. Another example of a successful replacement of carbon atoms by silicon atoms is silicon polyprismanes. Silicon polyprismanes are nanotubes of a particular type, built from silicon rings. It was found that such nanostructures exhibit unique metallic properties [18]. Also, in [19] the geometrical structure and nuclear magnetic resonance (NMR) parameters of the pristine, as well as carbon-, silicon-, and germanium-doped (10,0) boron nitride (BN) nanotubes, have been studied using a DFT/B3LYP method for the first time. It was found that the NMR parameters are significantly changed for those B and N nuclei that bond directly to C, Si, or a Ge dopant. Thus, compounds based on silicon and germanium may have unusual characteristics, and the substitution of carbon atoms leads to improving the properties of such systems. This approach is also applied to CL-20 molecules [20,21].

In this paper, density functional theory simulations were performed to predict the stability, energetic performance, and the physical and chemical properties of the CL-20 systems, wherein carbon atoms are replaced by silicon or germanium atoms. Density functional theory (DFT) is one of the most accurate methods to identify molecules' specifications and characteristics and is widely used in modern calculations to determine the properties of carbon systems. For example, in [22], the electronic, magnetic, and optical properties of graphene in the presence of Fe impurities and vacancies are demonstrated using DFT calculation within GGA. It has been found that the conductive property of graphene remains in the presence of Fe atoms and vacancies in the graphene structure. Furthermore, in [23], the authors study the influence of intermolecular interactions on the properties of carbon nanotubes using DFT. The DFT calculations are consistent with experimental data and predict the stability of the systems considered in Ref. [23]. In [24], the molecular adsorption of hydrogen sulfide was investigated theoretically by using density functional theory for gallium (Ga)-, germanium (Ge)-, and boron (B)-doped (4,0) single-walled carbon nanotubes.

Thus, the abbreviated names of systems in the present work are $\text{Si}_n\text{CL-20}/\text{Ge}_n\text{CL-20}$, where n is the number of substituted atoms, $n = 1, \dots, 6$. The fully silicon and germanium substituted molecules $\text{Si}_6\text{CL-20}/\text{Ge}_6\text{CL-20}$ are depicted in Figure 1b,c. We explained how the physicochemical properties of systems, such as the binding energy, HOMO–LUMO gap, chemical potential, and others depend on the number of silicon or germanium atoms added to the system instead of carbon. Furthermore, we estimated the cage strain energy of the classical CL-20 molecule using the design of homodesmotic reactions, as well as the effect of the substitution of carbon atoms by silicon and germanium atoms in the compound on this value.

2. Computational Details

The structural optimization and characterization of the $\text{Si}_n\text{CL-20}/\text{Ge}_n\text{CL-20}$ systems were carried out with the framework of density functional theory (DFT). Density functional theory is a basic method for the analysis of the properties of low-dimensional nanostructures with highly strained frameworks [25,26] and has been successful in terms of computing speed and accuracy [27].

All DFT calculations for the silicon/germanium analogues of the high-energy molecule CL-20 and its dimers were performed using the TeraChem software [28–31]. The traditional Becke's three-parameter hybrid method and the Lee–Yang–Parr exchange–correlation energy functional (B3LYP) [32,33] with the Pople basis set 6-311G(d,p) [34] were used for the calculations.

During geometry optimization, the global charge of all of the systems considered was neutral. The maximum force and root mean square forces were 4.5×10^{-4} and 3×10^{-4} (hartrees per bohr and hartrees per radian), whereas the maximum displacement and root mean square displacement were 1.8×10^{-3} and 1.2×10^{-3} . Mulliken charges were calculated at the same B3LYP/6-311G(d,p) level of theory. According to a benchmarking study [35], the typical error of energies of high-strained molecules calculated with the used DFT method is about 0.1 eV, and errors in bond lengths are smaller than 0.01 Å [36].

3. Results and Discussion

3.1. Geometry Optimization

First of all, we considered the pure unsubstituted CL-20 molecule, and then we began to replace carbon atoms with silicon or germanium atoms. We constructed several types of $\text{Si}_n\text{CL-20}/\text{Ge}_n\text{CL-20}$ molecules, where $n = 1, \dots, 6$ is the number of silicon/germanium atoms in the system that replaced the carbon atoms ($n = 0$ for traditional CL-20). It should be noted that the structure and geometry of the $\text{Si}_n\text{CL-20}/\text{Ge}_n\text{CL-20}$ molecule change strongly with the appearance of Si- or Ge-atoms in it. It can be seen in Figure 2, wherein the transformations of a pure molecule CL-20 into a fully silicon-substituted molecule $\text{Si}_6\text{CL-20}$ (a) or a fully germanium-substituted molecule $\text{Ge}_6\text{CL-20}$ are shown (b).

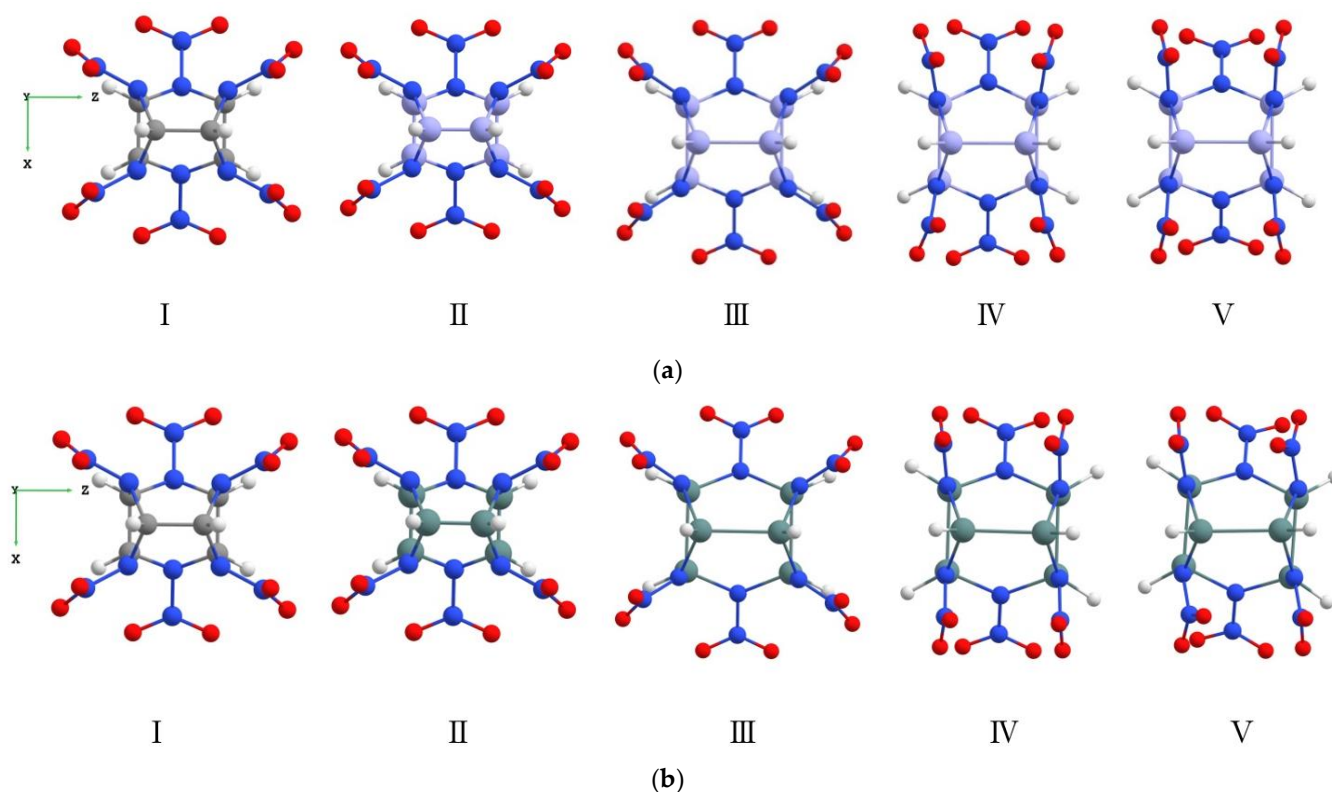


Figure 2. (a) From pure CL-20 to substituted $\text{Si}_6\text{CL-20}$; (b) From pure CL-20 to substituted $\text{Ge}_6\text{CL-20}$. I—The isolated molecule CL-20 (top view); II—the isolated non-optimized molecule $\text{Si}_6\text{CL-20}/\text{Ge}_6\text{CL-20}$ (Si-/Ge-atoms replaced all C-atoms); III, IV—optimization steps of $\text{Si}_6\text{CL-20}/\text{Ge}_6\text{CL-20}$ (increase in diameter and rotation of functional groups NO_2); V—the isolated optimized molecule $\text{Si}_6\text{CL-20}/\text{Ge}_6\text{CL-20}$. The color codes of the atoms are the same as in Figure 1.

The main difference between a pure molecule CL-20 and silicon or germanium molecules $\text{Si}_n\text{CL-20}/\text{Ge}_n\text{CL-20}$ is that the functional groups NO_2 make a significant rotation (Figure 2a,b) relative to the initial position in the classic molecule (Figure 2aI), and the effective diameter of the framework of the systems increases with the addition of Si-/Ge-atoms.

Table 1 shows the effective diameters for the most thermodynamically stable systems obtained at the B3LYP/6-311G(d,p) level of theory (see the next section for more information on the thermodynamic stability of systems). The effective diameter of the nanostructures was determined by us with the following formula

$$D_{\text{eff}} = \frac{\sum_{i=1}^{48} r_i}{48}, \quad (1)$$

where r_i is the distances between atoms in the carbon–germanium–nitrogen frame (we took into consideration four maximum distances for each of the 12 atoms included in the carbon–germanium–nitrogen framework of the molecule).

Table 1. The effective diameters D_{eff} (Å) of $\text{Si}_n\text{CL-20}/\text{Ge}_n\text{CL-20}$ obtained at the DFT/B3LYP/6-311G(d,p) level of theory.

n	0	1	2	3	4	5	6
$\text{Si}_n\text{CL-20}$	3.208	3.363	3.498	3.646	3.803	3.960	4.125
$\text{Ge}_n\text{CL-20}$		3.401	3.556	3.743	3.934	4.142	4.357

From Table 1, one can see that, when silicon or germanium atoms are added to the system, the effective diameter of the framework increases. It should be noted that an increase in the effective diameter is more significant for germanium-substituted molecules.

Besides, the average bond lengths between carbon, nitrogen, and silicon/germanium atoms, which are part of the framework of the most thermodynamically stable compounds $\text{Si}_n\text{CL-20}/\text{Ge}_n\text{CL-20}$ ($n = 1, \dots, 6$), were measured. These data are presented in Tables 2 and 3.

Table 2. The average bond lengths of the most thermodynamically stable compounds $\text{Si}_n\text{CL-20}$ obtained at the DFT/B3LYP/6-311G(d,p) level of theory. A dash “-” means that this bond is not found in the compound.

n	C–C, Å	C–N, Å	C–Si, Å	Si–Si, Å	Si–N, Å
0	1.590	1.461	-	-	-
1	1.591	1.461	1.938	-	1.778
2	1.589	1.465	1.941	-	1.778
3	-	1.469	1.944	-	1.779
4	-	1.467	1.940	2.393	1.787
5	-	1.467	1.948	2.372	1.792
6	-	-	-	2.379	1.795

Table 3. The average bond lengths of the most thermodynamically stable compounds $\text{Ge}_n\text{CL-20}$ obtained at the DFT/B3LYP/6-311G(d,p) level of theory. A dash “-” means that this bond is not found in the compound.

n	C–C, Å	C–N, Å	C–Ge, Å	Ge–Ge, Å	Ge–N, Å
0	1.590	1.461	-	-	-
1	1.589	1.460	2.029	-	1.892
2	1.590	1.455	-	2.474	1.902
3	1.593	1.459	2.012	2.473	1.903
4	1.604	1.462	-	2.445	1.914
5	-	1.452	2.017	2.476	1.903
6	-	-	-	2.481	1.903

3.2. Energy Properties

For understanding the energy efficiency and thermodynamic stability of the nanostructures, the binding energies E_b of classic CL-20 and $\text{Si}_n\text{CL-20}/\text{Ge}_n\text{CL-20}$ systems for all possible configurations with $n = 1, \dots, 6$ silicon or germanium atoms (that replaced the carbon atoms in the traditional CL-20 molecule) were obtained and analyzed. The binding energy E_b of the nanostructure per atom is determined by the equation

$$E_b \left[\frac{\text{eV}}{\text{atom}} \right] = \frac{1}{N_{\text{at}}} \{ iE(\text{H}) + kE(\text{O}) + lE(\text{N}) + mE(\text{C}) + nE(\text{Si/Ge}) - E_{\text{tot}}(\text{Si}_n\text{CL-20}/\text{Ge}_n\text{CL-20}) \} \quad (2)$$

where $N_{\text{at}} = i + k + l + m + n = 36$ is the total number of atoms in the system ($i = 6$; $k = 12$; $l = 12$; $m + n = 6$); $E_{\text{tot}}(\text{Si}_n\text{CL-20}/\text{Ge}_n\text{CL-20})$ is the total $\text{Si}_n\text{CL-20}/\text{Ge}_n\text{CL-20}$ nanostructure energy; and $E(\text{H})$, $E(\text{O})$, $E(\text{N})$, $E(\text{C})$, $E(\text{Si/Ge})$ are the energies of the isolated hydrogen, oxygen, nitrogen, carbon, and silicon/germanium atoms, respectively.

The system with higher binding energy (lower potential energy) is more thermodynamically stable and vice versa. The binding energies E_b obtained for all possible configurations $\text{Si}_n\text{CL-20}/\text{Ge}_n\text{CL-20}$, where n is the number of germanium atoms in the system ($n = 1,$

... ,6), are presented in Figure 3. The values of the binding energies for all such systems considered can be found in the Supplementary Materials (Tables S1 and S2). The point $n = 0$ corresponds to a pure unsubstituted CL-20 molecule. It can be seen that the addition of silicon/germanium atoms to the system leads to a decrease in the binding energy. Even for $n = 1$, the binding energy is quite noticeably different from the binding energy of a traditional CL-20 molecule. However, it has been established that the framework maintains stability with an increase in the number of substituting silicon or germanium atoms.

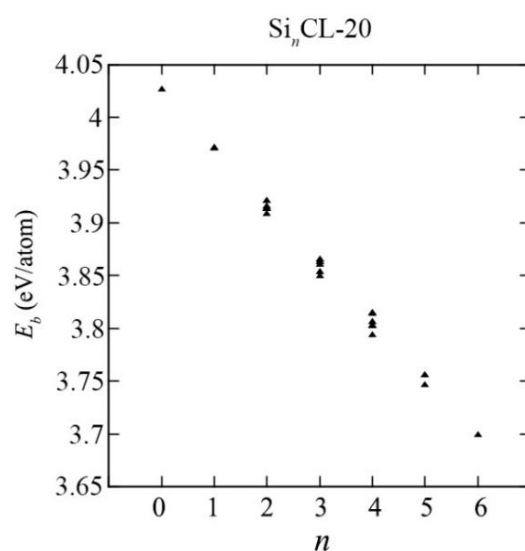


Figure 3. The binding energy versus the number of Si-atoms n in the Si_nCL-20 molecule for all possible configurations obtained at the DFT/B3LYP/6-311(d,p) level of theory.

As evident from Figures 3 and 4, as the number of Si-/Ge-atoms n in the Si_nCL-20/Ge_nCL-20 molecule increases, the value of the binding energy becomes smaller. Moreover, for germanium-substituted Ge_nCL-20 molecules, the decrease in the binding energy is sharper than that of silicon-substituted Si_nCL-20 , and for the same number of substituted atoms n , the binding energy of the germanium molecule is less than the corresponding value for the silicon molecule.

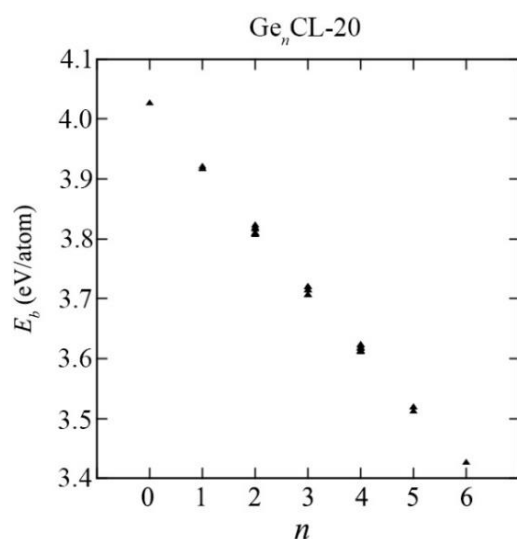


Figure 4. The binding energy versus the number of Ge-atoms n in the Ge_nCL-20 molecule for all possible configurations obtained at the DFT/B3LYP/6-311(d,p) level of theory.

For the same number of substituted atoms, the binding energy E_b of the systems is slightly different for various combinations of such atoms. For further consideration in this study, a combination with the maximum binding energy E_b was chosen for each number of substituted atoms n , since such systems are the most thermodynamically stable (see Figure 5).

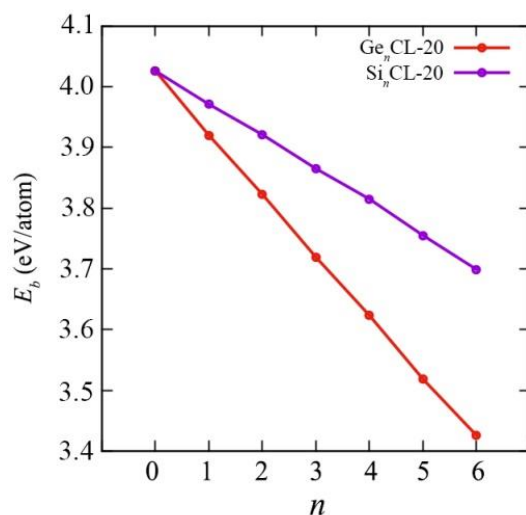


Figure 5. The binding energy versus the number of Si-/Ge-atoms n in the $\text{Si}_n\text{CL-20}/\text{Ge}_n\text{CL-20}$ molecule for the most thermodynamically stable configurations obtained at the DFT/B3LYP/6-311(d,p) level of theory.

For the maximum binding energies of germanium and silicon CL-20, using the least-squares method, linear regression equations were obtained depending on the number of substituted atoms $n=0, \dots, 6$:

$$E_b(\text{Si}_n\text{CL-20}) = -0.054n + 4.0273, \quad (3)$$

$$E_b(\text{Ge}_n\text{CL-20}) = -0.1001n + 4.0226. \quad (4)$$

Thus, we determined all further characteristics specifically for these most thermodynamically stable configurations for each value of Si-/Ge-atoms n , because these atomic arrangements are most beneficial. In addition, the data obtained for all possible types of arrangement of the silicon/germanium and carbon atoms in the skeleton of the molecules $\text{Si}_n\text{CL-20}/\text{Ge}_n\text{CL-20}$ for each number of substituted atoms n separately are presented in the Supplementary Materials (Tables S1 and S2).

3.3. Electronic Characteristics

To assess the potential use of the $\text{Ge}_n\text{CL-20}$ nanostructures in various electronic applications, the HOMO–LUMO gaps of such systems were determined. The HOMO–LUMO gap Δ_{HL} is defined as the energy gap between the highest occupied molecular orbital and the lowest unoccupied molecular orbital. The obtained results for HOMO–LUMO gaps of the most thermodynamically stable systems are presented in Figure 6. The HOMO and LUMO energies themselves of all $\text{Si}_n\text{CL-20}/\text{Ge}_n\text{CL-20}$ nanostructures considered can be found in the Supplementary Materials (Tables S1 and S2).

As is evident from Figure 6, the HOMO–LUMO gap for the $\text{Si}_1\text{CL-20}$ and $\text{Ge}_1\text{CL-20}$ molecules (5.923 eV and 5.814 eV, respectively) is slightly larger than the corresponding value for the unsubstituted CL-20 molecule (5.693 eV). However, when more carbon atoms are replaced by silicon or germanium atoms, the gap size decreases. However, a uniform decrease in this value is violated at $n = 4$. For example, for germanium systems, the $\text{Ge}_4\text{CL-20}$ molecule is characterized by the smallest HOMO–LUMO gap equal to 5.318 eV, while, for silicon systems, at $n = 4$, there is a sharp jump up to 5.580 eV.

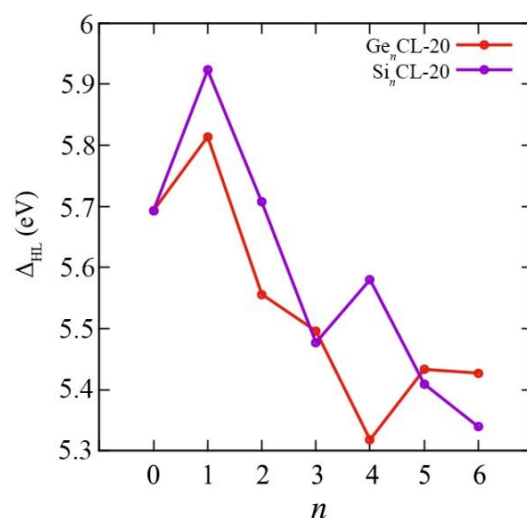


Figure 6. The HOMO–LUMO gap versus the number of Si-/Ge-atoms n in the $\text{Si}_n\text{CL-20}/\text{Ge}_n\text{CL-20}$ molecule for the most thermodynamically stable configurations obtained at the DFT/B3LYP/6-311(d,p) level of theory.

Mulliken charge analysis reveals that the largest charge is concentrated on silicon/germanium and nitrogen atoms of the $\text{Si}_n\text{CL-20}/\text{Ge}_n\text{CL-20}$ nanostructure. The greatest positive charge accumulates on silicon/germanium atoms and the greatest negative charge accumulates on nitrogen atoms belonging to the carbon-silicon/germanium-nitrogen framework. Therefore, the caged silicon/germanium atoms are favorable sites for a nucleophilic reaction, whereas the caged nitrogen atoms are a good target for an electrophilic reaction.

3.4. Chemical Reactivity Indices

Density functional theory was used in this study for the analysis of the chemical reactivity indices of the compounds and for obtaining a set of physical quantities, such as the electron affinity (EA) [37,38] first ionization potential (IP) [37,38], chemical hardness (η) [39] and softness (S) [38], chemical potential (μ) [40], electronegativity (χ) [41,42], and the electrophilicity index (ω) [40], which are linked to their electronic structure. The chemical potential, hardness, and electronegativity are defined as follows

$$\mu = \left(\frac{\partial E}{\partial N} \right)_v \quad (5)$$

$$\eta = \frac{1}{2} \left(\frac{\partial^2 E}{\partial N^2} \right)_v = \frac{1}{2} \left(\frac{\partial \mu}{\partial N} \right)_v' \quad (6)$$

$$\chi = -\mu = - \left(\frac{\partial E}{\partial N} \right)_v' \quad (7)$$

where E and v are the electronic energy and the constant external potential of an N -electron system. As one can see from Equation (6), chemical hardness is the resistance of the chemical potential to change in the number of electrons, i.e., it describes the resistance of the system to exchanging an electronic charge with the environment [38]. The concept of electronegativity was introduced by Pauling as the power of an atom in a molecule to attract an electron to it. To calculate these parameters, the Koopmans' theorem for closed-shell molecular systems was used [43]. According to this theorem, the ionization potential and electron affinity can be defined as the negative of the highest occupied molecular orbital (HOMO) ε_H and lowest unoccupied molecular orbital (LUMO) ε_L energy, respectively. Electron affinity refers to the capacity of the molecular systems to accept one electron from a donor, while the ionization potential refers to the ability of a molecular system to lose

electrons. Thus, the use of the finite difference approximation and Koopmans' theorem leads to the following expression for the chemical potential

$$\mu = -\frac{1}{2}(\text{IP} + \text{EA}) = \frac{1}{2}(\varepsilon_{\text{L}} + \varepsilon_{\text{H}}). \quad (8)$$

In addition, hardness can be calculated as

$$\eta = \frac{1}{2}(\varepsilon_{\text{L}} - \varepsilon_{\text{H}}) = \frac{1}{2}\Delta_{\text{HL}}, \quad (9)$$

where $\Delta_{\text{HL}} = \varepsilon_{\text{L}} - \varepsilon_{\text{H}}$ is the HOMO-LUMO gap. Note that the maximum electronic charge that the system can accept is $\Delta N_{\text{max}} = -\mu/\eta$ [40]. Softness is logically the reciprocal of hardness [38]

$$S = \frac{1}{2\eta}. \quad (10)$$

The electrophilicity concept was proposed by Parr and co-workers, and the electrophilicity index is defined in [40]

$$\omega = \frac{\mu^2}{2\eta}. \quad (11)$$

The electrophilicity index measures the stabilization in energy when the system acquires an additional electronic charge from the environment. According to Parr, an analog can be drawn between Equation (11) and the equation for power in classical electricity. Thus, the electrophilicity index can be described as some kind of "electrophilic power". Since electronegativity is the additive inverse of the chemical potential, the electrophilicity index can be also written as

$$\omega = \frac{\chi^2}{2\eta}. \quad (12)$$

We obtained all above mentioned quantum-chemical descriptors for the pure CL-20 and the $\text{Si}_n\text{CL-20}/\text{Ge}_n\text{CL-20}$, $n = 1, \dots, 6$. The chemical reactivity parameters are very important indices because they illustrate the reactivity and stability of the compounds. Chemical potential (μ), electronegativity (χ), hardness (η), and the electrophilicity index (ω) of the most thermodynamically stable configurations of $\text{Si}_n\text{CL-20}/\text{Ge}_n\text{CL-20}$ are presented in Figures 7–10, respectively. More complete data can be found in the Supplementary Materials (Tables S1 and S2).

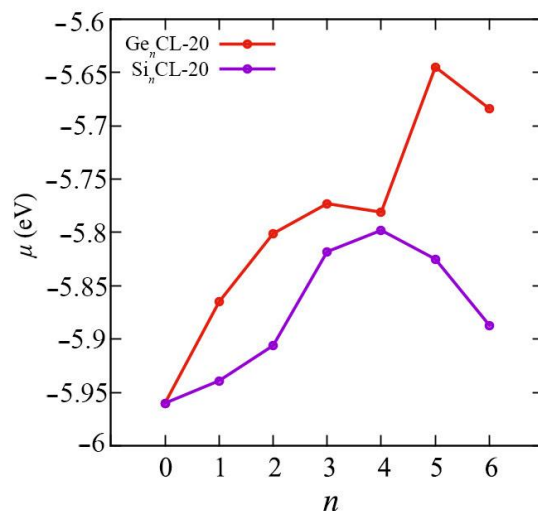


Figure 7. The chemical potential μ versus the number of Si-/Ge-atoms n in the $\text{Si}_n\text{CL-20}/\text{Ge}_n\text{CL-20}$ molecules for the most thermodynamically stable configurations obtained at the DFT/B3LYP/6-311(d,p) level of theory.

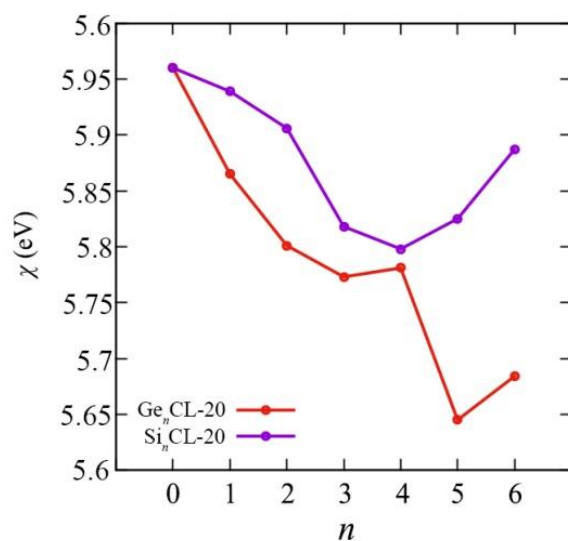


Figure 8. The electronegativity χ versus the number of Si-/Ge-atoms n in the $\text{Si}_n\text{CL-20}/\text{Ge}_n\text{CL-20}$ molecules for the most thermodynamically stable configurations obtained at the DFT/B3LYP/6-311(d,p) level of theory.

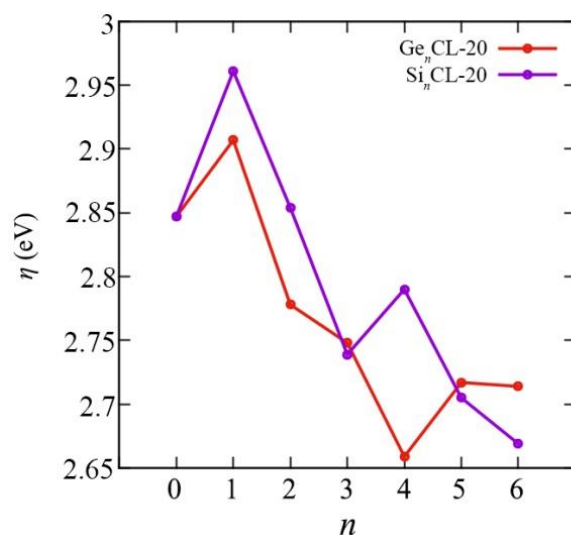


Figure 9. The hardness η versus the number of Si-/Ge-atoms n in the $\text{Si}_n\text{CL-20}/\text{Ge}_n\text{CL-20}$ molecules for the most thermodynamically stable configurations obtained at the DFT/B3LYP/6-311(d,p) level of theory.

The electronic chemical potential μ characterizes the change in energy when electrons are added to the molecular system, in other words, when the electron density changes. As can be seen from Figure 7, the chemical potential generally rises with the number of substituted atoms n in the $\text{Ge}_n\text{CL-20}$ system, and for $\text{Si}_n\text{CL-20}$ systems, it increases to $n = 4$ and then begins to decrease. Since electronegativity χ is defined as the electron chemical potential μ , the opposite picture is observed in Figure 8. Thus, with an increase in the number of Ge atoms n , the $\text{Ge}_n\text{CL-20}$ molecule is less able to attract an electron charge. The smooth monotonic dependence is broken for $n = 4$ and $n = 6$, so that the chemical potential μ for $\text{Ge}_4\text{CL-20}$ and $\text{Ge}_6\text{CL-20}$ is -5.781 eV and -5.684 eV, respectively. For silicon-substituted systems, the $\text{Si}_4\text{CL-20}$ molecule is the least capable of attracting an electronic charge; the chemical potential for it is -5.798 eV.

Furthermore, chemical hardness generally decreases with an increasing number of Si/Ge atoms in the system. Therefore, we can say that systems with a large number of

germanium atoms are less able to resist a change in electron density for a given change in chemical potential compared to pure CL-20, and a small change in the electron density of the system leads to a smaller change in chemical potential. In this regard, the isolated CL-20 molecule is the most stable in this regard ($\eta = 2.907$ eV), whereas, with an increase in the number of germanium atoms, $\text{Ge}_n\text{CL-20}$ nanostructures become more susceptible to changes in the electronic configuration, except for the case $n = 1$, when the graph experiences a sharp jump. The least stable in this sense is the $\text{Ge}_4\text{CL-20}$ system ($\eta = 2.659$ eV). For silicon systems, a smooth decay is also broken for $n = 4$.

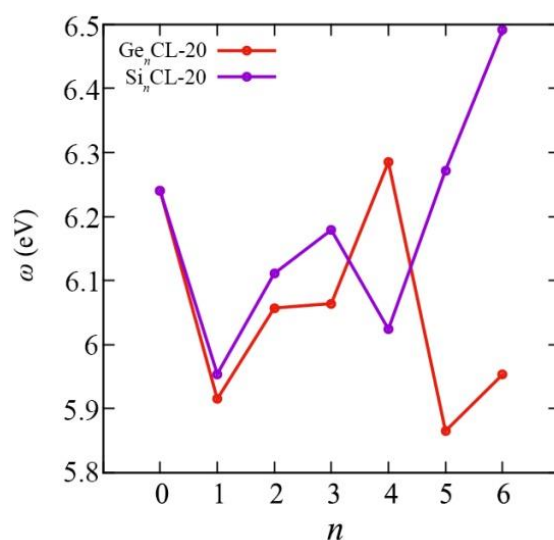


Figure 10. The electrophilicity ω versus the number of Si-/Ge-atoms n in the $\text{Si}_n\text{CL-20}/\text{Ge}_n\text{CL-20}$ molecules for the most thermodynamically stable configurations obtained at the DFT/B3LYP/6-311(d,p) level of theory.

In addition, it is difficult to establish the exact dependence of electrophilicity on the number of substituted Si-/Ge-atoms; however, analysis of this value shows that $\text{Ge}_4\text{CL-20}$ (among germanium-substituted systems) and $\text{Si}_6\text{CL-20}$ (among silicon-substituted systems) molecules have the highest level of energy stabilization when the system receives an additional charge from the environment.

3.5. The CL-20-Based Dimers

In this study, we considered dimers consisting of two CL-20 fragments or their silicon and germanium-substituted analogues, interconnected by CH_2 functional groups. For the balance between kinetic and thermodynamic stability, the $\text{Si}_5\text{CL-20}/\text{Ge}_5\text{CL-20}$ systems were chosen as the derivatives of the CL-20 molecule [21]. Three modifications of such systems were considered, that is, three types of compounds in the fragments of which five silicon or germanium atoms replaced carbon atoms at different positions. The studied systems are shown in Figure 11.

The binding energy E_b of the classical CL-20 dimer, as well as silicon and germanium dimers from $\text{Si}_5\text{CL-20}/\text{Ge}_5\text{CL-20}$ fragments, is determined by the equation

$$E_b \left[\frac{\text{eV}}{\text{atom}} \right] = \frac{1}{N_{\text{at}}} \{iE(\text{H}) + kE(\text{O}) + lE(\text{N}) + mE(\text{C}) + nE(\text{Si/Ge}) - E_{\text{tot}}\}, \quad (13)$$

where $N_{\text{at}} = i + k + l + m + n = 66$ is the total number of atoms in the system ($i = 16$; $k = 16$; $l = 20$; $m = 4$; $n = 10$); E_{tot} is the total energy of the dimer; $E(\text{H})$, $E(\text{O})$, $E(\text{N})$, $E(\text{C})$, $E(\text{Si/Ge})$ are the energies of the isolated hydrogen, oxygen, nitrogen, carbon, and silicon/germanium atoms, respectively.

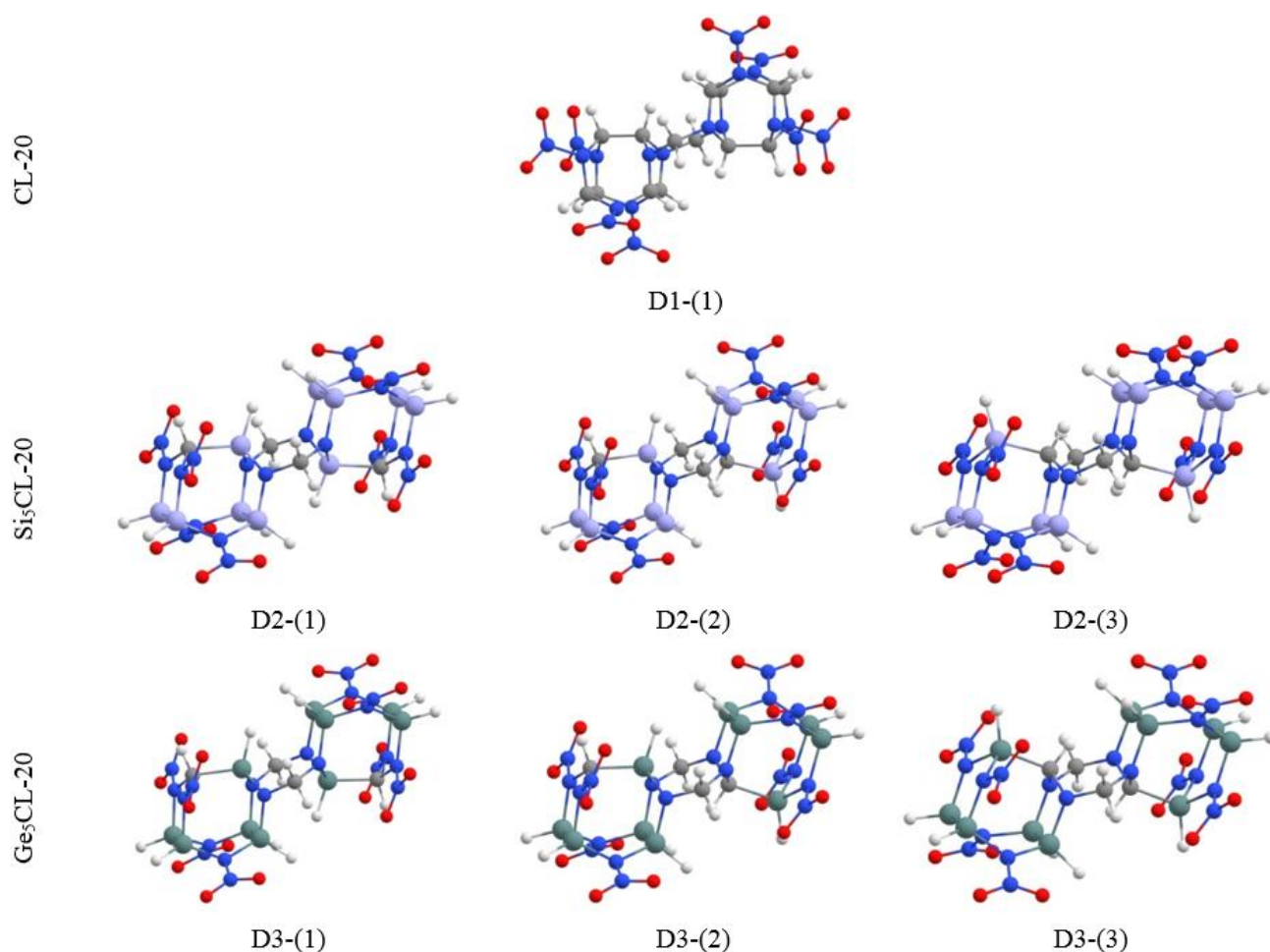


Figure 11. D1-(1)—the dimer of pure molecules CL-20; D2-(1), D2-(2), D2-(3)—the dimers of silicon molecules Si₅CL-20; D3-(1), D3-(2), D3-(3)—the dimers of germanium molecules Ge₅CL-20.

The values of the binding energy E_b obtained for the dimers are presented in Table 4. It can be seen that the addition of silicon and germanium atoms to the system leads to a decrease in the binding energy. Thus, the classical CL-20 dimer is more thermodynamically stable compared to its substituted analogues. However, silicon and germanium nanostructures remain stable in this regard.

Table 4. The binding energies, HOMO–LUMO gaps, ϵ_H and ϵ_L energies of the dimers based on CL-20, Si₅CL-20, and Ge₅CL-20 molecules obtained at the DFT/B3LYP/6-311(d,p) level of theory.

The Dimer		E_b , eV/atom	ϵ_H , eV	ϵ_L , eV	Δ_{HL} , eV
	D1-(1)	4.156	−7.454	−2.797	4.657
Si	Si-D2-(1)	3.843	−7.489	−3.031	4.458
	Si-D2-(2)	3.843	−7.478	−3.061	4.462
	Si-D2-(3)	3.846	−7.609	−2.293	4.715
Ge	Ge-D3-(1)	3.579	−7.181	−2.771	4.410
	Ge-D3-(2)	3.579	−7.124	−2.780	4.345
	Ge-D3-(3)	3.582	−7.167	−2.793	4.374

Dimers based on Ge₅CL-20 fragments with different types of arrangements of silicon or germanium atoms have close binding energies. Therefore, we can conclude that the

arrangement of silicon and germanium atoms in the framework does not strongly affect the thermodynamic stability of the dimer.

The results for HOMO–LUMO gaps, as well as the energy of the highest occupied molecular orbital (HOMO) ϵ_H and the smallest unoccupied molecular orbital (LUMO) ϵ_L systems, are presented in Table 4.

The value of the HOMO–LUMO gap for silicon dimers D2-(1) and D2-(2) is close and less than the corresponding value for the unsubstituted CL-20 dimer. However, for the D2-(3) dimer, on the contrary, the HOMO–LUMO gap is large. For germanium dimers, the HOMO–LUMO gap value is less than the corresponding value for a classical dimer. At the same time, the HOMO–LUMO gaps of germanium dimers differ slightly among themselves. It is assumed that, when building larger systems based on pure CL-20 fragments and their silicon or germanium derivatives, the difference will be more significant. Details on the electronic properties and chemical activity data can be found in the Supplementary Materials (Table S3).

3.6. Homodesmotic Reactions and Strain Energies

Compounds in the form of a cage or a ring usually have a high density, and, at the same time, they release a lot of energy when the framework opens. Thus, it is reasonable to evaluate the stability of high-energy compounds from the point of view of the frame deformation energy. The strain of the framework of the compound is associated with the changes in bond distances and bond angles or rotational conformations about the normal hybridization state of the atoms in a molecule [44–46]. Cage strain energy makes a great contribution to the power of high-energy compounds. Furthermore, the higher the strain energy characterizing the deformation of the framework, the more unstable the molecule behaves and the more difficult it is to synthesize experimentally [44]. Thus, studies of the strain energy of the cage may be useful for the synthesis of high-energy compounds based on the CL-20 molecule. Strain energy can be defined as the difference between energies for a process that releases strain as determined by the experiment and as obtained from a model that does not involve strain [47].

In this work, we considered several homodesmotic reactions to calculate the strain energies of the high-energy molecule CL-20 and its substituted derivatives. Homodesmotic reactions are a refinement of isodesmic reactions [48] and have been extensively used to calculate strain energy E_s [47,49–53]. In a homodesmotic reaction, the number of bonds of different types and the valence medium around each atom are preserved. The advantage of using a homodesmotic reaction is that the cancellation of errors, associated with the truncation of the basis sets and incomplete electron correlation recovery, occurs to a large extent [49,50]. Thus, the previous studies showed that the theoretically predicted values of E_s in homodesmotic reactions were in good agreement with the experiments [49,52].

The homodesmotic reaction (Figure 12), previously presented in [44], was used to calculate the strain energies (E_s) of the cells of classical hexanitrohexaazaisowurtzitane CL-20. The same reactions were used to obtain these characteristics for its silicon- and germanium-substituted analogues $\text{Si}_6\text{CL-20}/\text{Ge}_6\text{CL-20}$, but carbon atoms were replaced by silicon or germanium atoms in all reactants and reaction products.

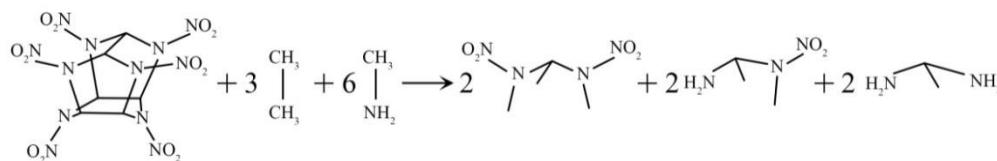


Figure 12. The homodesmotic reaction used to obtain the strain energy of CL-20 framework.

Thus, the cage strain energy can be expressed as [38,54]

$$E_s = E_{\text{tot}}(\text{reactants}) - E_{\text{tot}}(\text{products}), \quad (14)$$

where E_s is the strain energy, $E_{tot}(reactants)$ is the total energy of the reactants at 0 K, and $E_{tot}(products)$ is the total energy of the reaction products at 0 K. We ignored the zero-point energies and thermal energy increases ongoing above 0 K. All strain energy values, as well as the total energies of the compounds involved in the homodesmotic reaction necessary for calculation, are presented in Table 5.

Table 5. The strain energies E_s of CL-20/Si₆CL-20/Ge₆CL-20 molecules obtained from homodesmotic reactions (14) at the DFT/B3LYP/6-311(d,p) level of theory.

Molecule	CL-20	Si ₆ CL-20	Ge ₆ CL-20
E_s , eV	2.843	1.474	2.039

Framework strain energy can reflect the thermal stability of high-energy compounds. The higher the strain energy, the more unstable the molecule, and a compound with high cage strain energy is difficult to experimentally synthesize. However, strain is not really a measure of thermodynamic stability, because by itself it does not give a value of the enthalpy or the free energy change for any particular reaction but rather affords a feel for the energy released when the reaction has occurred [54]. An increase of cage strain energy may result in a decrease in stability, but more energy will release when a cage opening occurs [44].

An estimate of the strain energies for a pure CL-20 molecule and its silicon and germanium analogues Si₆CL-20/Ge₆CL-20 obtained by homodesmotic reactions shows that the addition of silicon or germanium atoms to the system leads to a decrease in the value of this energy. It indicates that, when the framework of a pure CL-20 molecule opens, most of the energy will be released. Thus, the classical molecule is the most energy-efficient.

4. Conclusions

In this work, we studied isolated silicon- and germanium-substituted CL-20 systems and also performed a comparative analysis of their properties compared to a pure unsubstituted CL-20 molecule. Dimers built from the classical CL-20 molecules and their silicon and germanium derivatives Si₅CL-20/Ge₅CL-20 were also studied. The energy and electronic properties of Si_nCL-20 and Ge_nCL-20 systems with carbon atoms replaced by silicon/germanium atoms and their dimers were investigated using the B3LYP/6-311G(d,p) level of theory. The addition of silicon/germanium atoms to the system leads to a decrease in the binding energy. However, it has been established that the framework maintains stability with an increase in the number of substituting silicon or germanium atoms. We estimated the value of the strain energy for a CL-20 molecule and its substituted derivatives Si₆CL-20/Ge₆CL-20 using homodesmotic reactions and ab initio calculations. It was found that, for a classical pure molecule, more energy will be released when the framework is broken than when the substituted derivatives decay. In this sense, a pure molecule is the most energy-efficient. Therefore, in the future, it is possible to use the studied data of the considered silicon and germanium derivatives of the CL-20 molecule for constructing covalent crystals based on them. The substituted silicon and germanium CL-20 molecules are promising materials since they can be used as a basis for high-energy materials and fuels. The synthesis of such materials is a rather difficult task; therefore, attempts to synthesize new CL-20 molecules should be preceded by comprehensive theoretical studies. Thus, we hope this study will attract more interest from synthesis researchers to explore these compounds.

Supplementary Materials: The following supporting information can be downloaded at: <https://www.mdpi.com/article/10.3390/ma15196577/s1>, Table S1: binding energy and descriptors of reactivity of Si_nCL-20 molecule; Table S2: binding energy and descriptors of reactivity of Ge_nCL-20 molecule; Table S3: binding energies and descriptors of reactivity of covalent dimers based on CL-20, Ge₅CL-20, and Si₅CL-20 molecules. Figure S1: The isolated molecule Si₆CL-20 with numbered silicon atoms. Figure S2: The isolated molecule Ge₆CL-20 with numbered silicon atoms.

Author Contributions: Conceptualization, M.M.M.; data curation, M.A.G., M.M.M. and K.P.K.; formal analysis, M.A.G., M.M.M. and K.P.K.; funding acquisition, M.M.M. and K.P.K.; investigation, M.A.G., M.M.M. and K.P.K.; methodology, M.A.G., M.M.M. and K.P.K.; project administration, M.M.M. and K.P.K.; resources, M.A.G., M.M.M. and K.P.K.; software, M.A.G.; supervision, M.M.M.; validation, M.A.G., M.M.M. and K.P.K.; visualization, M.A.G.; writing—original draft, M.A.G.; writing—review and editing, M.M.M. and K.P.K. All authors have read and agreed to the published version of the manuscript.

Funding: This work was supported by the MEPhI program Priority 2030.

Institutional Review Board Statement: Not applicable.

Informed Consent Statement: Not applicable.

Data Availability Statement: The data is available as Supplementary Materials to this article.

Conflicts of Interest: The authors declare no conflict of interest.

References

1. Sysolyatin, S.V.; Lobanova, A.A.; Chernikova, Y.T.; Sakovich, G.V. Methods of synthesis and properties of hexanitrohexaazaisowurtzitane. *Russ. Chem. Rev.* **2005**, *74*, 757–764. [[CrossRef](#)]
2. Klapötke, T.M. *High Energy Density Materials*; Springer: Berlin/Heidelberg, Germany, 2007.
3. Hang, G.; Yu, W.; Wang, T.; Wang, J. Theoretical investigations into effects of adulteration crystal defect on properties of CL-20/TNT cocrystal explosive. *Comput. Mater. Sci.* **2019**, *156*, 77–83. [[CrossRef](#)]
4. Tan, J.-J.; Ji, G.-F.; Chen, X.-R.; Li, Z. Structure, equation of state and elasticity of crystalline HNIW by molecular dynamics simulations. *Phys. B Condens. Matter* **2011**, *406*, 2925–2930. [[CrossRef](#)]
5. Zhou, G.; Wang, J.; He, W.-D.; Wong, N.-B.; Tian, A.; Li, W.-K. Theoretical investigation of four conformations of HNIW by B3LYP method. *J. Mol. Struct. THEOCHEM* **2002**, *589–590*, 273–280. [[CrossRef](#)]
6. Kozlova, S.A.; Gubin, S.A.; Maklashova, I.V.; Selezenev, A.A. Molecular-dynamic simulations of the thermophysical properties of hexanitrohexaazaisowurtzitane single crystal at high pressures and temperatures. *Russ. J. Phys. Chem. A* **2017**, *91*, 2157–2160. [[CrossRef](#)]
7. McBain, A.; Vuppuluri, V.; Gunduz, I.E.; Groven, L.J.; Son, S.F. Laser ignition of CL-20 (hexanitrohexaazaisowurtzitane) cocrystals. *Combust. Flame* **2018**, *188*, 104–115. [[CrossRef](#)]
8. Zhou, J.-H.; Shi, L.-W.; Zhang, C.-Y.; Li, H.-Z.; Chen, M.-B.; Chen, W.-M. Theoretical analysis of the formation driving force and decreased sensitivity for CL-20 cocrystals. *J. Mol. Struct.* **2016**, *1116*, 93–101. [[CrossRef](#)]
9. Sha, Y.; Zhang, X. Impact sensitivity and moisture adsorption on the surface of CL-20/TNT cocrystal by molecular dynamics simulation. *Appl. Surf. Sci.* **2019**, *483*, 91–97. [[CrossRef](#)]
10. Wu, C.; Zhang, S.; Gou, R.; Ren, F.; Han, G.; Zhu, S. Theoretical insight into the effect of solvent polarity on the formation and morphology of 2,4,6,8,10,12-hexanitrohexaazaisowurtzitane (CL-20)/2,4,6-trinitro-toluene(TNT) cocrystal explosive. *Comput. Theor. Chem.* **2018**, *1127*, 22–30. [[CrossRef](#)]
11. Liu, K.; Zhang, G.; Luan, J.; Chen, Z.; Su, P.; Shu, Y. Crystal structure, spectrum character and explosive property of a new cocrystal CL-20/DNT. *J. Mol. Struct.* **2016**, *1110*, 91–96. [[CrossRef](#)]
12. Hang, G.; Yu, W.; Wang, T.; Wang, J.; Li, Z. Theoretical insights into effects of molar ratios on stabilities, mechanical properties and detonation performance of CL-20/RDX cocrystal explosives by molecular dynamics simulation. *J. Mol. Struct.* **2017**, *1141*, 577–583. [[CrossRef](#)]
13. Katin, K.P.; Maslov, M.M. Toward CL-20 crystalline covalent solids: On the dependence of energy and electronic properties on the effective size of CL-20 chains. *J. Phys. Chem. Solids* **2017**, *108*, 82–87. [[CrossRef](#)]
14. Gimaldinova, M.A.; Maslov, M.M.; Katin, K.P. Electronic and reactivity characteristics of CL-20 covalent chains and networks: A density functional theory study. *CrystEngComm* **2018**, *20*, 4336–4344. [[CrossRef](#)]
15. Kan, S.B.J.; Lewis, R.D.; Chen, K.; Arnold, F.H. Directed evolution of cytochrome c for carbon–silicon bond formation: Bringing silicon to life. *Science* **2016**, *354*, 1048–1051. [[CrossRef](#)] [[PubMed](#)]
16. Showell, G.A.; Mills, J.S. Chemistry challenges in lead optimization: Silicon isosteres in drug discovery. *Drug Discov. Today* **2003**, *8*, 551–556. [[CrossRef](#)]
17. Jones, R.G.; Ando, W.; Chojnowski, J. *Silicon-Containing Polymers: The Science and Technology of Their Synthesis and Applications*; Springer Science & Business Media: Berlin/Heidelberg, Germany, 2000. [[CrossRef](#)]
18. Gimaldinova, M.A.; Katin, K.P.; Salem, M.A.; Maslov, M.M. Energy and electronic characteristics of silicon polyprismanes: Density functional theory study. *Lett. Mater.* **2018**, *8*, 454–457. [[CrossRef](#)]
19. Ahmadi, T.S.; Seif, A.; Rozbahani, G.M. The pristine and carbon, silicon or germanium-substituted (10,0) BN nanotube: A computational DFT study of NMR parameters. *Arabian J. Chem.* **2010**, *3*, 121–126. [[CrossRef](#)]
20. Tan, B.; Huang, H.; Huang, M.; Long, X.; Li, J.; Yuan, X.; Xu, R. Computational screening of several silicon-based high-energy hexanitrohexaazaisowurtzitane-like derivatives. *J. Fluor. Chem.* **2014**, *158*, 29–37. [[CrossRef](#)]

21. Katin, K.P.; Javan, M.B.; Kochaev, A.I.; Soltani, A.; Maslov, M.M. Kinetic Stability and Reactivity of Silicon and Fluorine-Containing CL-20 Derivatives. *ChemistrySelect* **2019**, *4*, 9659–9665. [[CrossRef](#)]
22. Ostovari, F.; Hasanpoori, M.; Abbasnejad, M.; Salehi, M.A. DFT calculations of graphene monolayer in presence of Fe dopant and vacancy. *Phys. B Condens. Matter* **2018**, *541*, 6–13. [[CrossRef](#)]
23. Kamedulski, P.; Kaczmarek-Kedziera, A.; Lukaszewicz, J.P. Influence of intermolecular interactions on the properties of carbon nanotubes. *Bull. Mater. Sci.* **2018**, *41*, 76. [[CrossRef](#)]
24. Gecim, G.; Ozekmekci, M. A density functional theory study of molecular H₂S adsorption on (4,0) SWCNT doped with Ge, Ga and B. *Surf. Sci.* **2021**, *711*, 121876. [[CrossRef](#)]
25. Javan, M.B. Electronic transport properties of linear nC₂₀ (n ≤ 5) oligomers: Theoretical investigation. *Phys. E* **2015**, *67*, 135–142. [[CrossRef](#)]
26. Strout, H.D.L. Stability of Carbon–Nitrogen Cages in Fourfold Symmetry. *J. Phys. Chem. A* **2006**, *110*, 4089–4092. [[CrossRef](#)] [[PubMed](#)]
27. Parr, R.G.; Yang, W. *Density-Functional Theory of Atoms and Molecules*; Oxford University Press: New York, NY, USA, 1989.
28. Ufimtsev, I.S.; Martínez, T.J. Quantum Chemistry on Graphical Processing Units. 3. Analytical Energy Gradients, Geometry Optimization, and First Principles Molecular Dynamics. *J. Chem. Theory Comput.* **2009**, *5*, 2619–2628. [[CrossRef](#)] [[PubMed](#)]
29. Titov, A.V.; Ufimtsev, I.S.; Luehr, N.; Martínez, T.J. Generating Efficient Quantum Chemistry Codes for Novel Architectures. *J. Chem. Theory Comput.* **2013**, *9*, 213–221. [[CrossRef](#)] [[PubMed](#)]
30. Kästner, J.; Carr, J.M.; Keal, T.W.; Thiel, W.; Wander, A.; Sherwood, P. DL-FIND: An Open-Source Geometry Optimizer for Atomistic Simulations. *J. Phys. Chem. A* **2009**, *113*, 11856–11865. [[CrossRef](#)] [[PubMed](#)]
31. Goumans, T.P.M.; Catlow, C.R.A.; Brown, W.A.; Kästner, J.; Sherwood, P. An embedded cluster study of the formation of water on interstellar dust grains. *Phys. Chem. Chem. Phys.* **2009**, *11*, 5431–5436. [[CrossRef](#)] [[PubMed](#)]
32. Lee, C.; Yang, W.; Parr, R.G. Development of the Colle-Salvetti correlation-energy formula into a functional of the electron density. *Phys. Rev. B* **1988**, *37*, 785–789. [[CrossRef](#)]
33. Becke, A.D. Density-functional thermochemistry. III. The role of exact exchange. *J. Chem. Phys.* **1993**, *98*, 5648–5652. [[CrossRef](#)]
34. Krishnan, R.; Binkley, J.S.; Seeger, R.; Pople, J.A. Self-consistent molecular orbital methods. XX. A basis set for correlated wave functions. *J. Chem. Phys.* **1980**, *72*, 650–654. [[CrossRef](#)]
35. Guner, V.; Khuong, K.S.; Leach, A.G.; Lee, P.S.; Bartberger, M.D.; Houk, K.N. A Standard Set of Pericyclic Reactions of Hydrocarbons for the Benchmarking of Computational Methods: The Performance of ab Initio, Density Functional, CASSCF, CASPT2, and CBS-QB3 Methods for the Prediction of Activation Barriers, Reaction Energetics, and Transition State Geometries. *J. Phys. Chem. A* **2003**, *107*, 11445–11459. [[CrossRef](#)]
36. Amin, E.A.; Truhlar, D.G. Zn Coordination Chemistry: Development of Benchmark Suites for Geometries, Dipole Moments, and Bond Dissociation Energies and Their Use To Test and Validate Density Functionals and Molecular Orbital Theory. *J. Chem. Theory Comput.* **2008**, *4*, 75–85. [[CrossRef](#)] [[PubMed](#)]
37. Foresman, J.B.; Frisch, A.E. *Exploring Chemistry with Electronic Structure Methods*, 2nd ed.; Gaussian Inc.: Pittsburgh, PA, USA, 1996.
38. Lewars, E.G. *Computational Chemistry: Introduction to the Theory and Applications of Molecular and Quantum Mechanics*; Kluwer Academic Publishers: Norwell, MA, USA, 2003.
39. Pearson, R.G. Absolute electronegativity and hardness correlated with molecular orbital theory. *Proc. Natl. Acad. Sci. USA* **1986**, *83*, 8440–8441. [[CrossRef](#)]
40. Parr, R.G.; Szentpaly, L.V.; Liu, S. Electrophilicity Index. *J. Am. Chem. Soc.* **1999**, *121*, 1922–1924. [[CrossRef](#)]
41. Putz, M.V.; Russo, N.; Sicilia, E. Atomic radii scale and related size properties from density functional electronegativity formulation. *J. Phys. Chem. A* **2003**, *107*, 5461–5465. [[CrossRef](#)]
42. Parr, R.G.; Donnelly, R.A.; Levy, M.; Palke, W.E. Electronegativity: The density functional viewpoint. *J. Chem. Phys.* **1978**, *68*, 3801–3807. [[CrossRef](#)]
43. Koopmans, T. Über die zuordnung von wellenfunktionen und eigenwerten zu den einzelnen elektronen eines atoms. *Physica* **1933**, *1*, 104–113. [[CrossRef](#)]
44. Tan, B.; Long, X.; Li, J. The cage strain energies of high-energy compounds. *Comput. Theor. Chem.* **2012**, *993*, 66–72. [[CrossRef](#)]
45. Schleyer, P.V.R.; Williams, J.E.; Blanchard, K.R. Evaluation of strain in hydrocarbons. The strain in adamantane and its origin. *J. Amer. Chem. Soc.* **1970**, *92*, 2377–2386. [[CrossRef](#)]
46. Wiberg, K.B. The concept of strain in organic chemistry. *Angew. Chem. Int. Ed.* **1986**, *25*, 312–322. [[CrossRef](#)]
47. Zhao, M.; Gimarc, B.M. Strain energies in cyclic oxygen O_n, n = 3–8. *J. Phys. Chem.* **1993**, *97*, 4023–4030. [[CrossRef](#)]
48. Hehre, W.J.; Radom, L.; Schleyer, P.V.R.; Pople, J.A. *Ab Initio Molecular Orbital Theory*; Section 6.5.6; Wiley-Interscience: New York, NY, USA, 1985.
49. Walker, J.E.; Adamson, P.A.; Davis, S.R. Comparison of calculated hydrocarbon strain energies using ab initio and composite methods. *J. Mol. Struct. THEOCHEM* **1999**, *487*, 145–150. [[CrossRef](#)]
50. Fan, X.-W.; Qiu, L.; Ju, X.-H. Cage strain in nitro-substituted 1,3,5,7-tetraazacubanes. *Struct. Chem.* **2009**, *20*, 1039–1042. [[CrossRef](#)]
51. Fan, X.-W.; Ju, X.-H. Theoretical studies on four-membered ring compounds with NF₂, ONO₂, N₃, and NO₂ groups. *J. Comput. Chem.* **2007**, *29*, 505–513. [[CrossRef](#)]

-
52. Lewis, L.L.; Turner, L.L.; Salter, E.A.; Magers, D.H. Computation of the conventional strain energy in oxaziridine. *J. Mol. Struct. THEOCHEM* **2002**, *592*, 161–171. [[CrossRef](#)]
 53. George, P.; Trachtman, M.; Bock, C.W.; Brett, A.M. An alternative approach to the problem of assessing destabilization energies (strain energies) in cyclic hydrocarbons. *Tetrahedron* **1976**, *32*, 317–322. [[CrossRef](#)]
 54. Lewars, E.G. *Modeling Marvels. Computational Anticipation of Novel Molecules*; Springer Science & Business Media: Berlin/Heidelberg, Germany, 2008; p. 242. [[CrossRef](#)]